Optics Letters

Bragg reflective polychromatic vector beam generation from opposite-handed cholesteric liquid crystals

Tiegang Lin,[1] Yide Yuan,[1] Yaqin Zhou,[1] Wenxing Fu,[1] Huihui Huang,[1] Lishuang Yao,[2] Fan Fan,[1,*] and Shuangchun Wen[1]

[1]Key Laboratory for Micro/Nano Optoelectronic Devices of Ministry of Education & Hunan Provincial Key Laboratory of Low-Dimensional Structural Physics and Devices, School of Physics and Electronics, Hunan University, Changsha 410082, China
[2]State Key Laboratory of Applied Optics, Changchun Institute of Optics, Fine Mechanics and Physics, Chinese Academy of Sciences, Changchun 130033, China
*Corresponding author: ffan@hnu.edu.cn

Received 19 March 2019; revised 25 April 2019; accepted 25 April 2019; posted 29 April 2019 (Doc. ID 362730); published 23 May 2019

In this Letter, a method of stacking two opposite-handed cholesteric liquid crystals (CLCs) with the same pitches and the same surface azimuthal angles to generate vector beams from homogeneous linear polarization is proposed. By this means, vector beams with arbitrary orders can be generated based on point-to-point photo-alignment technology. In our experiment, radially polarized, azimuthally polarized, and high-order vector beams with high efficiency have been generated. The device operates light polarization within the Bragg reflection polychromatic bandgap. Our proposal also provides the possibility to generate reflective hybrid-order Poincaré beams if these two CLC layers are impressed with different topological charges. It has great potential for reflective photonics applications in high-resolution imaging, focusing, and information processing.

https://doi.org/10.1364/OL.44.002720

Vector beams, such as radially or azimuthally polarized light, known as having the space-variant polarizations in the transverse plane have attracted much attention in recent years, because they have many potential uses in optical communication and information technologies. Many applications based on the generation and manipulation of vector beams can be developed, including high-numerical aperture focusing, high-resolution imaging, nanoparticle manipulation, laser machining, remote sensing, and quantum information processing [1–3].

Various generation methods for obtaining vector beams have been reported and can be distinguished into two types. One type generates the vector beams in a direct way via laser intracavity devices; nevertheless, most of the devices require rigorous alignment or special fabrication techniques [4]. Other methods for generating beams were proposed in a passive way via converting the homogeneously polarized beams into desired inhomogeneous polarizations outside the laser cavity, including liquid crystal (LC) devices, subwavelength gratings, and plasmonics or dielectric metasurfaces [5–15]. Among them, LC devices are more popular, since they have the advantages in fabrication, efficiency, price, convenience, and tuning by electric, temperature, light, or other external stimuli. To date, twist nematic LC cells, LC q-plates, as well as spatial light modulators based on nematic LC materials, are used to generate vector beams [5–8]. Today, with the development of nanoscaled point-to-point photo-alignment and nanoimprinting technology, spatial-variant retardation axis arrangements for quarter-wave plates or half-wave plates can realize the transformation from circular or linear polarization to complex polarization distribution, respectively [9,10]. Unfortunately, the approaches mentioned above can only operate the light at a specific single wavelength. Although twist nematic LC cells can realize the broadband light polarization transformation at the Mauguin condition, the cell gap is thick which is not advantageous to electrical driving [5,10].

Cholesteric liquid crystals (CLCs), as anisotropic and stratified media, have the selectivity of circularly polarized light in a Bragg reflective region, when the wavelength at normal incidence satisfies the condition: $n_o p < \lambda < n_e p$, where n_e and n_o are the extraordinary and ordinary refractive indices of LC material, and the pitch p is the distance over which the director twists 2π. Based on the above remarkable phenomena, many applications were developed, including filters, circular polarizers, displays, and lasers [16–19]. Recently, the reflective Bragg-Berry phase elements, such as vortex beam generators, flat lenses, and beam splitters, were disclosed, since the geometric phase effect was acquired from the light reflected by the periodic structure of the anisotropic medium [20–25]. However, flipping the incident circular polarization state does not imply the Berry phase reversal. The fundamental limitation prevents the generation of vector beams from homogeneous linear polarization based on a CLC device with monotonous chirality.

In this Letter, we overcome the limitation and propose that CLCs can be also used to realize the polarization conversion in a robust and direct way. It is demonstrated that light beams with

homogenous linear polarization can be transformed into inhomogeneous polarization distribution via reflecting off the two opposite-handed CLC stacking layers. It is benefited from the polarization selection feature of the CLC. Moreover, the three-dimensional self-assemble superstructure can be reconfigurable by point through a digital micro-mirror device (DMD) to align the polarization-sensitive alignment agent.

A σ handed circularly polarization state propagating along the z-axis can be expressed as $\vec{e}_\sigma = (\vec{x} + \sigma i\vec{y})/\sqrt{2}$, where $\sigma = \pm 1$ implies the sign of photon spin angular momentum projection to the positive direction of z-axis. On the one hand, circularly polarized light of the same handedness as the helix of CLC is reflected for propagating towards the helix axis in Bragg bandgap. The reflected light conserves its polarization, and a Berry phase $\Phi_B = 2\sigma\theta_s$ is obtained, where σ is the handedness of input circular polarization, and θ_s is the orientation angle of LC molecules with the x-axis in the front surface. As for circularly polarized input light expressed as $\vec{E}_{\text{in}} = E_0\vec{e}_\sigma \exp i(kz - \omega t)$, the reflected light can be formulated into $\vec{E}_r = E_0\vec{e}_{-\sigma} \exp(i\Phi_B) \exp i(-wt - kz)$. On the other hand, the circularly polarized light with opposite handedness is transmitted through the CLC medium, and the transmitted light conserves its polarization and cannot lead to the Berry phase.

Here we use two CLC layers with opposite handedness to generate vector beams. The LC molecules were designed as seen in Fig. 1(a). The blue and cyan parts represent right-handed CLC (RCLC) and left-handed CLC (LCLC), respectively. There is a physical space made by the glass between the two layers. In the fixed reference coordinate system (x, y, z), the directors at the front and end surfaces of the two layers are orientated at an angle θ_s with the x-axis, and the directors at the surface can be anchored together in the experiment. The two CLC layers have the same pitches p and equal thickness d. The thickness of each layer is $n \times p$, where n is an integer

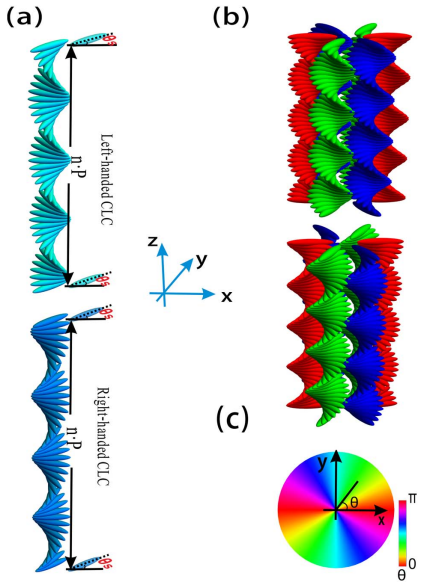

Fig. 1. (a) Right and left helix LC molecular arrays with orientation angle θ_s on the boundary surfaces. Schematic representation of the molecular orientation (b) in the bulk and (c) at the surfaces of the designed vector beam generation device with $q = 1$ and $\theta_0 = 0$.

or half-integer. In general, n is larger than 10, so that the Bragg reflection tends to show theoretical 100% efficiency. Input light propagates along the positive direction of the z-axis, first interacting with RCLC and then LCLC media. As for right-handed circularly polarized (RCP) incident light expressed as $\vec{E}_{\text{in}} = E_0([1, -i]^T/\sqrt{2}) \exp i(kz - \omega t)$, it is totally reflected by RCLC and the reflected light can be expressed as $\vec{E}_r = E_0([1, i]^T/\sqrt{2}) \exp(-2i\theta_s) \exp i(-kz - \omega t)$. As for left-handed circularly polarized (LCP) light, that is, $\vec{E}_{\text{in}} = E_0([1, i]^T/\sqrt{2}) \exp i(kz - \omega t)$, the light passes through the RCLC layer and then was reflected by LCLC media. The reflected light can be formulated into $\vec{E}_r = E_0([1, -i]^T/\sqrt{2}) \exp(i2\theta_s) \exp(i\Delta\varphi) \exp i(-kz - \omega t)$. Here the reflected light is still LCP, so that it can transmit through the RCLC layer. Note that $\Delta\varphi$ implies the dynamical phase difference caused by not only the optical path difference between the two orthogonal circularly polarized components, but also the phase of the reflection coefficient of the cholesteric layers. Because the difference between the distances they travelled is small, as compared with a Rayleigh diffraction length, the minor mismatch in beam sizes between RCP and LCP can be neglected, so that we can only consider the evolution of polarization and phase.

Based on two orthogonal circularly polarized states, the incident polarization along the x-direction can be expressed as $\vec{E}_{\text{in}} = ([1, i]^T + [1, -i]^T)/2$. According to the above analysis to the light interacting with anisotropic media shown in Fig. 1(a), the reflected light should be given by $\vec{E}_r = ([1, -i]^T \exp(2i\theta_s) \exp(i\Delta\varphi) + [1, i]^T \exp(-2i\theta_s))/2$. It can be further simplified into $\vec{E}_r = ([\cos(2\theta_s + \Delta\varphi/2), \sin(2\theta_s + \Delta\varphi/2)]^T) \exp i(\Delta\varphi/2)$. More generally, for incident linear polarization with $\vec{E}_{in} = [\cos\alpha, \sin\alpha]^T$ illuminating the device, the polarization direction of the output light field is described by $\vec{E}_{\text{out}} = [\cos(2\theta_s + \Delta\varphi/2 - \alpha), \sin(2\theta_s + \Delta\varphi/2 - \alpha)]^T$. The device behaves like a half-wave plate with a slow axis at an angle $\theta_s + \Delta\varphi/4$ [5].

If the optical axis on the surface is defined as $\theta_s = q\varphi + \theta_0$, where q is a constant specifying the topological charge, φ shows the azimuthal angle, and θ_o is a constant indicating the initial orientation on the x-axis, a reflective space-variant polarization-vortex beam would be generated via input light with homogeneous polarization interacting with the device. Based on the theory mentioned above, the polarization order is $P = 2q$, where P denotes the topological charge of the polarized light field. Moreover, $\Delta\varphi$ and θ_o influence the initial polarization direction. Figure 1(b) shows one of the cases of the three-dimensional space-variant molecular array with $q = 1$, $\theta_0 = 0$. Its optical axis on the surface is demonstrated in Fig. 1(c).

Figure 2 illustrates the optical process of generating the radially polarized beams from homogeneous linear polarization. The structure of the device, including photo-alignment layers, glass substrates, and RCLC and LCLC layers, can also be seen in this illustration.

First, RCLC/LCLC materials were prepared. They were mixed by nematic LC6200 and chiral agent R811/S811 at a ratio of 77:23 to ensure a central wavelength of 633 nm. Then we fabricated an empty cell with a dual gap and 10 μm spacers were used to define these two gaps. On each inner substrate surface, the photo-alignment materials SD1

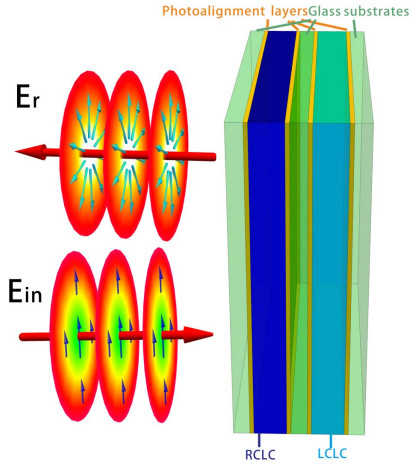

Fig. 2. Radially polarized beam generation process illustration. When the input light with homogeneous linear polarization first interacts with RCLC and LCLC layers with the topological charge $q = 1/2$. The reflected radially polarized light can be generated at a proper sample orientation.

(from Dainippon Ink and Chemicals Inc.) deposition was about 75 nm thick. Then the cell was exposed to DMD to reorient their absorption oscillators perpendicular to the ultraviolet light polarization. The excellent image output capability of the technique allows surface LC molecules to be orientated arbitrarily with the guide of SD1 molecules. After that, RCLC and LCLC materials were filled into the two empty gaps. Next, we used a spectrometer to analyze the reflectance corresponding to each wavelength from 500 to 800 nm which can be seen in Fig. 3. The black dotted line shows reflection spectrum of linearly polarized (LP) light source illuminating the device from the front side. The pink and green dotted lines show the reflection spectra of the RCP light source illuminating the device from the front side and back side, respectively. The blue and red dotted lines show the reflection spectra of LCP light source illuminating the device from the front side and back side, respectively. The front and back sides are close to the RCLC and LCLC layers, respectively. From the measured spectra, it can be seen that the Bragg reflection region ranges from 600 to 670 nm, and the reflectivity was nearly 100% efficiency for

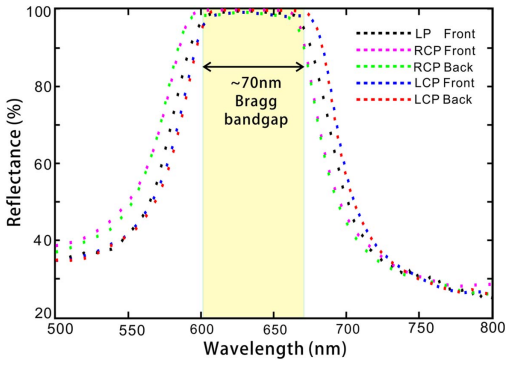

Fig. 3. Reflection spectra of a device at normal incidence when the LP source illuminates the device from the front side (black dotted line), RCP from the front side (pink dotted line) and back side (blue dotted line), and LCP from the front side (green dotted line) and back side (red dotted line).

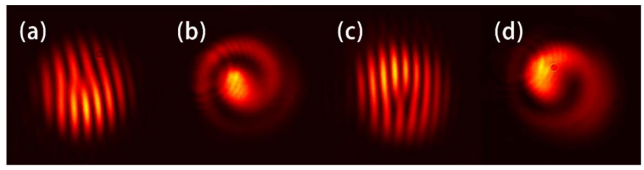

Fig. 4. (a) and (b) Measured interference profiles of the generated vortex beam with a plane wave and a spherical wave when RCP illuminated the device. (c) and (d) Measured interference patterns of the generated vortex beam with a plane wave and a spherical wave when LCP illuminated the device.

LP, RCP, and LCP sources. The central wavelength of the bandgap is 635 nm, and its width is about 70 nm. This indicates that RCLC and LCLC have remarkable circular polarization selectivity. In addition, the reflectivity for light illuminating from both sides is uniform. Here the substrates do not have any antireflection coating. The ~25% transmission loss is due to the reflections of the glass substrates.

With regard to the device with $q = 1/2$, when we use RCP light to illuminate the device, the process of spin-orbital angular momentum conversion is conducted by RCLC layer, and the topological charge of the orbital angular momentum is $l = -1$. The interference images of the reflective vortex beam with a plane wave and a spherical wave are measured, corresponding to Figs. 4(a) and 4(b). When LCP light is used as source, the process of spin-orbital angular momentum conversion is conducted by LCLC layer and the topological charge of the orbital angular momentum is $l = 1$. The corresponding interference images of reflective vortex beams with a plane wave and a spherical wave are represented in Figs. 4(c) and 4(d), respectively.

In our experiment, we control the ideal phase difference $\Delta\varphi = 2m\pi$ at 633 nm, and we use linearly polarized light in the x-direction to illuminate the device, where m is an integer. When $q = 1/2$, $\theta_0 = 0$, the reflective beam should be radially polarized. The polarized beams without analyzers exhibit ring-like intensity distribution profiles with dark centers, which can be seen in Fig. 5(a). Figures 5(b)–5(e) show the intensity pattern after the beams passing through the linear polarization analyzer with different orientations symbolized by white arrows. This reveals that the local polarization orientation is parallel to the corresponding axial direction. When $q = 1/2$, $\theta_0 = 45°$, the reflective beam should be azimuthally polarized. Similarly, Fig. 5(f) indicates the image of reflective vector beam. The polarization state of the beam can be checked with an

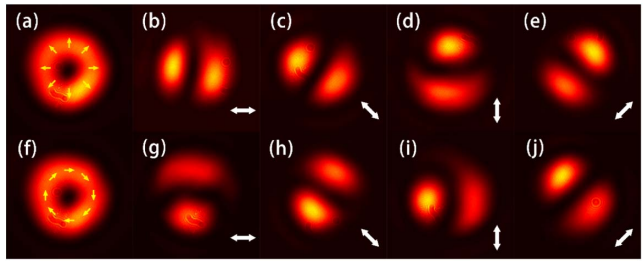

Fig. 5. Intensity distributions of (a)–(e) radially and (f)–(j) azimuthally polarized light recorded by a CCD camera. The white arrows represent the orientation of the linear analyzer.

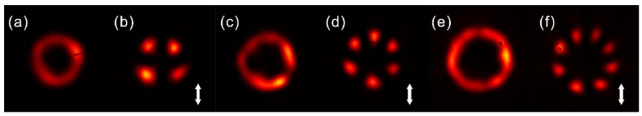

Fig. 6. Experimental intensity distributions of high-order vector beams with (a–b) $P = 2$, (c–d) $P = 3$, and (e–f) $P = 4$. The white arrows represent the orientation of the linear analyzer.

analyzer by the methods described above. The reflected beam profiles after passing through the analyzer can be seen in Figs. 5(g)–5(j). This reveals that the local polarization orientation is perpendicular to the corresponding axial direction. In fact, arbitrary cylindrical vector beams with $P = 1$ can be generated by changing the initial direction angle θ_0.

Further, we fabricated the devices with $q = 1, 1.5, 2$. The order number of the reflective vector beams should be $P = 2, 3, 4$. The reflected vector beams with $P = 2$ can be seen in Figs. 6(a) and 6(b). The reflected vector beams with $P = 3$ can be seen in Figs. 6(c) and 6(d). The reflected vector beams with $P = 4$ can be seen in Figs. 6(e) and 6(f). Figures 6(a), 6(c), and 6(e) are directly recorded by CCD cameras, and the corresponding beam images after passing through polarization analyzer are exhibited in Figs. 6(b), 6(d), and 6(f), respectively.

In summary, we theoretically and experimentally demonstrated that reflective vector beams can be generated via input light with homogeneous linear polarization interacting with two combined CLC layers with opposite handedness. In the experiment, traditional azimuthally and radially polarized beams, as well as high-order vector beams, are generated based on Bragg reflection. In this way, it also overcomes the limitation of CLC reflectivity [18,19]. The efficiency is nearly 100% in the polychromatic Bragg region. In addition, if the RCLC and LCLC were impressed with different topological charges, the reflective structured light beams on the hybrid-order Poincaré sphere will be generated. If we fill the opposite-handed CLC materials into the two gaps with different pitches, the dual-band spin-orbital angular momentum conversion device will be obtained. Therefore, the method provides more freedom on tuning reflectivity and bandgaps with regard to mirror-backed manner proposed in Ref. [26]. Moreover, RCLC and LCLC layers can be fabricated on a single glass substrate by polymer-stabilized or film-stacking technology [16,19] for reducing the volume of optical system and scattering. Furthermore, LC devices based on the point-to-point photo-alignment technology exhibit greater potential flexibility than rubbing alignment technology; hence, arbitrary-order and even multiple-order alternate polarization beams [10], can be generated with same fabrication process.

Funding. National Natural Science Foundation of China (NSFC) (11574079, 61605046, 61704053); Natural Science Foundation of Hunan Province (2018JJ3069); The State Key Laboratory of Applied Optics; Fundamental Research Funds for the Central Universities of China.

REFERENCES

1. Q. W. Zhan, Adv. Opt. Photonics **1**, 1 (2009).
2. K. S. Youngworth and T. G. Brown, Opt. Express **7**, 77 (2000).
3. R. Dorn, S. Quabis, and G. Leuchs, Phys. Rev. Lett. **91**, 233901 (2003).
4. M. A. Ahmed, J. Schulz, A. Voss, O. Parriaux, J. C. Pommier, and T. Graf, Opt. Lett. **32**, 1824 (2007).
5. M. Stalder and M. Schadt, Opt. Lett. **21**, 1948 (1996).
6. C. S. Guo, Z. Y. Rong, and S. Z. Wang, Opt. Lett. **39**, 386 (2014).
7. Z. Y. Rong, Y. J. Han, S. Z. Wang, and C. S. Guo, Opt. Express **22**, 1636 (2014).
8. X. L. Wang, J. Ding, W. J. Ni, C. S. Guo, and H. T. Wang, Opt. Lett. **32**, 3549 (2007).
9. F. Fan, T. Du, A. K. Srivastava, W. Lu, V. Chigrinov, and H. S. Kwok, Opt. Express **20**, 23036 (2012).
10. P. Chen, W. Ji, B. Y. Wei, W. Hu, V. Chigrinov, and Y. Q. Lu, Appl. Phys. Lett. **107**, 241102 (2015).
11. M. A. Ahmed, A. Voss, M. M. Vogel, and T. Graf, Opt. Lett. **32**, 3272 (2007).
12. Z. Bomzon, G. Biener, V. Kleiner, and E. Hasman, Opt. Lett. **27**, 285 (2002).
13. A. Arbabi, Y. Horie, M. Bagheri, and A. Faraon, Nat. Nanotechnol. **10**, 937 (2015).
14. Q. Guo, C. Schlickriede, D. Wang, H. Liu, Y. Xiang, T. Zentgraf, and S. Zhang, Opt. Express **25**, 14300 (2017).
15. Y. Q. Zhang, X. Y. Zeng, R. R. Zhang, Z. J. Zhan, X. Li, C. X. Liu, C. W. He, and C. F. Cheng, Opt. Lett. **43**, 4208 (2018).
16. Y. Huang, Y. Zhou, and S. T. Wu, Opt. Express **15**, 6414 (2007).
17. M. Mitov, Adv. Mater. **24**, 6260 (2012).
18. J. D. Lin, H. L. Lin, H. Y. Lin, G. J. Wei, Y. C. Chuang, L. J. Chen, S. Y. Huang, C. Y. Huang, T. S. Mo, and C. R. Lee, J. Mater. Chem. C **5**, 3222 (2017).
19. Y. Li, Y. J. Liu, H. T. Dai, X. H. Zhang, D. Luo, and X. W. Sun, J. Mater. Chem. C **5**, 10828 (2017).
20. J. Kobashi, H. Yoshida, and M. Ozaki, Nat. Photonics **10**, 389 (2016).
21. R. Barboza, U. Bortolozzo, M. G. Clerc, and S. Residori, Phys. Rev. Lett. **117**, 053903 (2016).
22. M. Rafayelyan, G. Tkachenko, and E. Brasselet, Phys. Rev. Lett. **116**, 253902 (2016).
23. J. Kobashi, H. Yoshida, and M. Ozaki, Phys. Rev. Lett. **116**, 253903 (2016).
24. M. Rafayelyan, G. Agez, and E. Brasselet, Phys. Rev. A **96**, 043862 (2017).
25. T. Lin, Y. Zhou, Y. Yuan, W. Fu, L. Yao, H. Huang, F. Fan, and S. Wen, Opt. Express **26**, 29244 (2018).
26. M. Rafayelyan and E. Brasselet, Phys. Rev. Lett. **120**, 213903 (2018).